Journal of BUON **14:** 103-108, 2009

ORIGINAL ARTICLE

A feasibility study on the use of digital tomosynthesis with individually-acquired megavoltage portal images for target localization

V. Sarkar, C. Shi, P. Rassiah-Szegedi, T. Eng, A. Diaz, N. Papanikolaou

Cancer Therapy and Research Center, University of Texas Health Science Center, San Antonio, TX, USA

Summary

Purpose: *To determine the feasibility of using megavoltage (MV) images and digital tomosynthesis to determine the three dimensional (3D) localization of different objects.*

Materials and methods: *Different phantom geometries were imaged using an electronic portal imaging device and digital tomosynthesis was used to reconstruct tomograms. These were compared with corresponding computed tomography (CT) images.*

Results: *While in-plane resolution of the tomograms was comparable as that of the CT images, definite out-of-plane (depth) localization was restricted to 5 mm.*

Conclusion: *The results confirm that it is possible to perform 3D localization of objects by using digital tomosynthesis for volumetric reconstructions from individually-acquired MV-quality portal images.*

Key words: localization, megavoltage, tomosynthesis

Introduction

With the advent of Intensity Modulated Radiation Therapy (IMRT) and the ability to produce dose distributions that are highly conformal to the tumor volume, correct patient positioning becomes of prime importance. Several approaches have been proposed to aid in this task, from the use of implanted radio frequency beacons [1-3] to the use of multi-planar or volumetric image sets, the latter technique leading to the field of Image Guided Radio Therapy (IGRT) [4-8]. Since we use a CT dataset for most radiotherapy planning, consistency can be maintained by using the same imaging modality when we are checking for positioning accuracy. With the recent developments in electronic portal imaging devices (EPIDs), there has been much work recently published in the field of cone-beam CT [9-12] using either the actual treatment beam or a kilovoltage (kV) beam from an x-ray tube attached to the gantry.

There are several implications with this approach, from the variation of machine output over the image set acquisition [13] to the time required for the whole acquisition, which may lead to some motion artifacts. While a lot of work has been done with modified linear accelerators or high efficiency receptors to obtain all the projection images required for a complete CT reconstruction [10], the implementation of this technique depends on specialized equipment. The typical clinic with a conventional linear accelerator requires a minimum of 1 monitor unit (MU) to acquire one projection image using an EPID. In that case, the dose that would be given to the patient for the acquisition of the 200 or so images required for a full CT reconstruction becomes too large to be acceptable. Indeed, a recent publication [14] highlighted some of the risks of high doses due to CT exams being carried out and, while the benefits of a CT being done for localization may outweigh the risks of missing part of the target, the general ALARA guidelines still require that we maintain the excess dose to a minimum. Our aim is to generate an image dataset that will mimic a CT dataset while only requiring a fraction of the images needed for CT reconstruction.

Correspondence to: Vikren Sarkar, Bs. 7979 Wurzbach Road, MC 7889/Radiation Oncology, San Antonio, TX 78229, USA. Tel: +1 210 450 1061, Fax: +1 210 616 5682, E-mail: sarkar@uthscsa.edu

Received 30-05-2008; Accepted 10-07-2008

The technique of tomosynthesis was first introduced in 1932 by Zeidses des Plantes [15] but it was the pioneering work of Garrison et al. [16], Miller et al. [17] and Grant [18] that showed its potentials as an imaging modality decades later. It is around that same time that the landmark research was being done on CT, leading to a relative loss of interest in tomosynthesis. However, with the recent development of high-efficiency digital receptors and the lower cost of computing power, the past decade has seen a renewed interest [19] in the imaging modality, with much of the work devoted to mammography [20-24] and, more recently, patient localization in radiotherapy [25-27]. However, most of this effort concentrates on using data using a kV beam. Two recent publications have looked at MV-tomosynthesis [28,29] but both used a linear accelerator already outfitted for conebeam CT reconstruction.

The purpose of this project was to determine the feasibility of using individually-acquired MV portal images acquired using a charge-coupled device (CCD) - based EPID as the source data to perform digital tomosynthesis (DTS) using only a software platform.

Materials and methods

For all the experiments performed for this project, a Theraview CCD-based EPID (Theraview Inc., Leusden, The Netherlands) mounted on a Varian clinic 2100 C/D (Varian Oncology, Palo Alto, CA) was used to acquire the portal images. These were then processed in an in-house developed program based on Matlab (version 7.0, The Mathworks Inc., Natick, MA) to perform DTS using the "shift-and-add" algorithm proposed by Kolitsi et al. [30]. The three different phantom configurations described next were used for different parts of the project.

Phantom configuration 1

For the first experiment, a phantom was created out of 4 layers of 1 cm thick bolus and steel washers. Figure 1 shows the construction of the phantom.

The phantom was positioned so that the linear accelerator's isocenter was in the middle of the phantom. A total of 9 images were acquired from 340° to 20° using a 5° interval with 5 MU per image. Tomograms were reconstructed using the following labeling scheme: a positive number was used to denote a slice that was above the isocenter while negative numbers were used to denote slices below the isocenter. The number used denotes the distance from isocenter in units of centimeter.

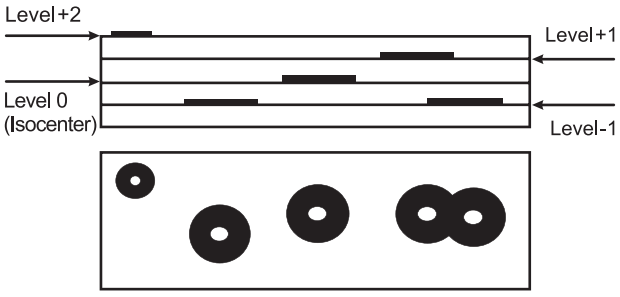

Figure 1. Geometry used for the tests. Steel washers were inserted between layers of 1 cm thick bolus. Both a side and top view are given.

Two further geometries were explored where small metallic markers were placed in different regions of an anthropomorphic Rando phantom (The Phantom Laboratory, Salem, NY). In each case, a MV CT data set was obtained using the Hi-Art II linear accelerator (Tomotherapy Inc., Madison, WI) at our clinic before moving the phantom to the Varian clinac to acquire EPID images. The phantom was positioned so that the isocenter of the linear accelerator was coincident to the location used as the imaging isocenter during MVCT acquisition. Portal images were subsequently obtained.

Phantom configuration 2

In the first experiment with the anthropomorphic phantom, small set screws (4 mm in diameter and 14 mm in length) were placed in the left breast of the Rando phantom. For this experiment, 4 total image sets were obtained. Two sets of portals were acquired at the same angles used for the first experiment, one using 1 MU per image and one using 5 MU per image. Two additional image sets were acquired from 70° to 110° at 5° intervals, once again using 1 MU and 5 MU per image. These two sets allowed for reconstruction of slices in the coronal and sagittal plane, respectively.

Phantom configuration 3

As a second experiment with the anthropomorphic phantom, gold seed markers (Civco Medical Solutions, Kalona, IA) with a diameter of 1.6 mm and length of 3 mm were positioned in the head of the Rando phantom. The same imaging protocol as for phantom 2 was used, except that images were only acquired with 1 MU.

Since the contrast between the metallic inserts and the surrounding tissue was low on the portal images, the DTS tomogram generated offered even lower contrast since they consist of the addition of shifted images. As a solution to this problem, we decided to

increase the contrast of the original portal images by manually highlighting the location of each insert using Microsoft Paint (Microsoft Corp, Redmond, WA) before DTS reconstruction was performed.

The ImageJ software (National Institute of Health, Bethesda, MD) was used to extract CT slices from the MV dataset and compared with the corresponding DTS slice.

Results

Phantom configuration 1

Figures 2 and 3 show the results of the first experiment where only coronal slices were reconstructed.

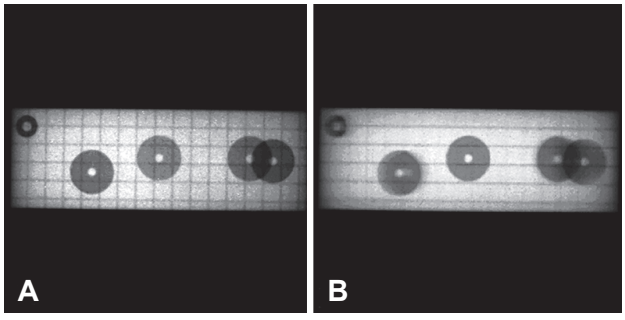

Figure 2. A: A single EPID projection image. **B:** Result of summing all EPID images without any shifts applied.

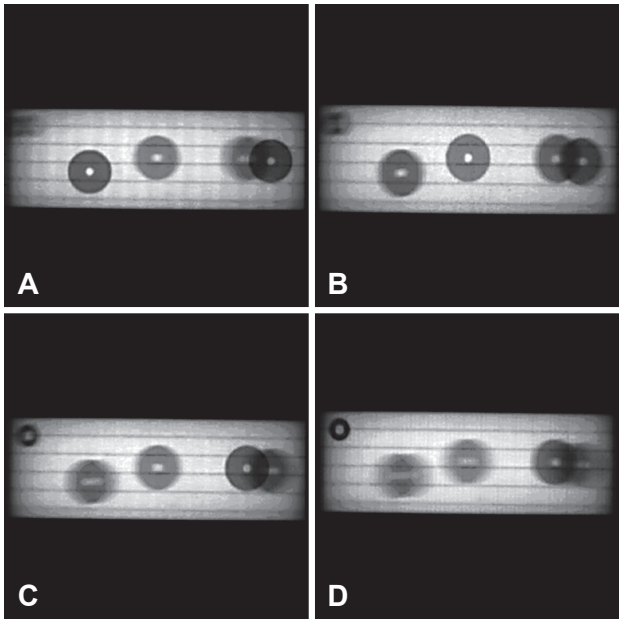

Figure 3. DTS reconstructions at levels -1 (**A**), 0 (**B**), +1 (**C**) and +2 (**D**).

Phantom configuration 2

Figures 4 and 5 compare corresponding coronal and sagittal CT and DTS images for the phantom with metallic inserts placed in the breast. Figure 6 compares two DTS images, one reconstructed from portals acquired with 1 MU and the other one using portals obtained using 5 MU.

Phantom configuration 3

Figure 7 shows two axial CT slices extracted from the CT dataset of the phantom. The labeling scheme used is the same to the one used for phantom 1. The top left image of Figure 8 shows what happens when

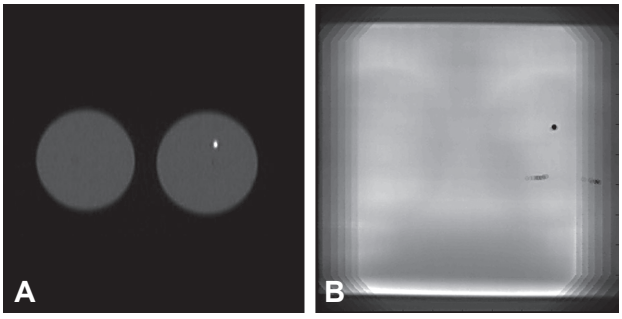

Figure 4. Corresponding CT (**A**) and DTS (**B**) slices for coronal reconstruction of phantom 2.

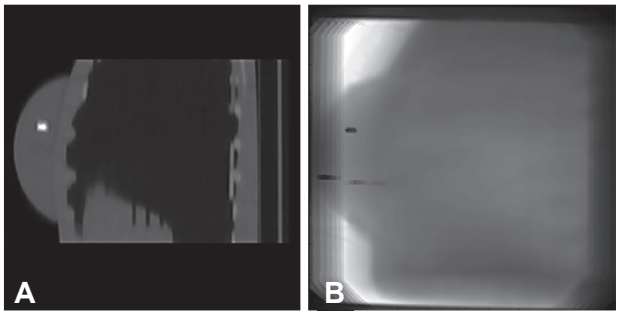

Figure 5. Corresponding CT (**A**) and DTS (**B**) slices for sagittal reconstruction of phantom 2.

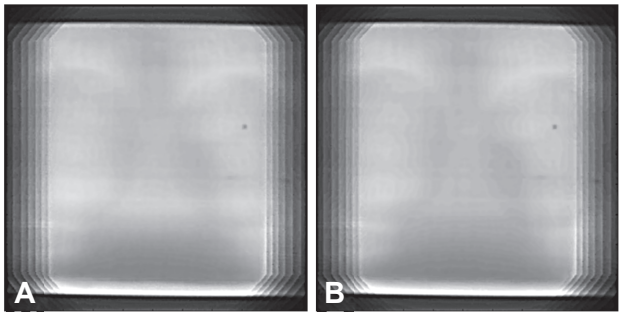

Figure 6. Coronal images of the same slice reconstructed from data acquired with 1 MU (**A**) and 5 MU (**B**).

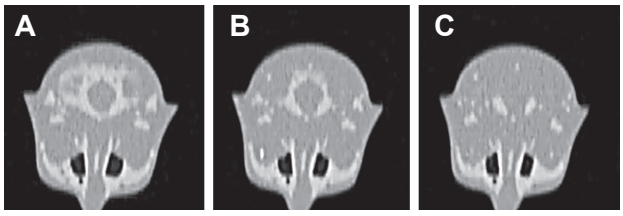

Figure 7. Coronal CT slices taken at level -1.8 cm (**A**), -2.0 cm (**B**) and -2.3 cm (**C**).

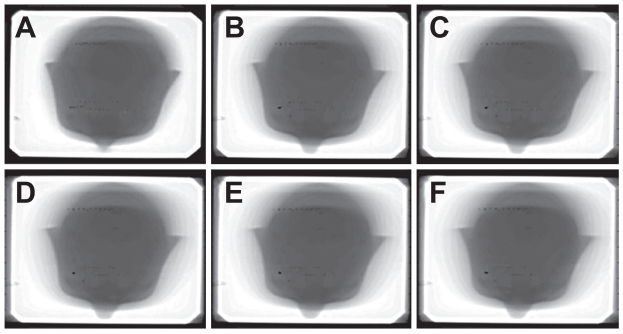

Figure 8. A – Figure obtained by addition of all EPID images without any shifting. **B-E** – DTS tomograms reconstructed at -1.5 cm (**B**), -1.8 cm (**C**), -2.0 cm (**D**), -2.3 cm (**E**) and -2.5 cm (**F**).

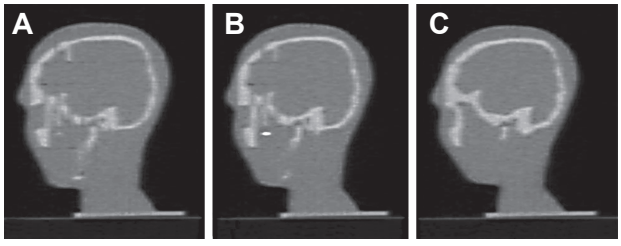

Figure 9. Sagittal CT slices taken at level -3.9 cm (**A**), -4.1 cm (**B**) and -4.2 cm (**C**).

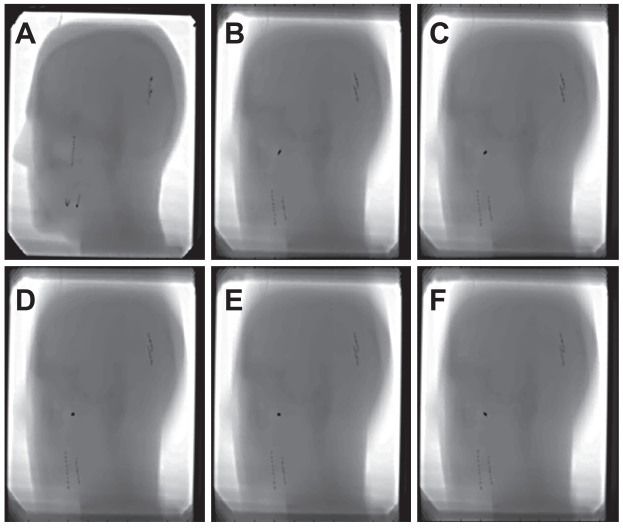

Figure 10. A – Figure obtained by addition of all EPID images without any shifting. **B-E** - DTS tomograms reconstructed at -3.7 cm (**B**), -3.9 cm (**C**), -4.1 cm (**D**), -4.2 cm (**E**) and -4.4 cm (**F**).

all portal images acquired are added with no shifting, while the other images show different DTS-based tomograms rebuilt using this data. Figures 9 and 10 show the corresponding images built as sagittal sections.

Discussion

Phantom configuration 1

A comparison between the various DTS images of Figure 3 and the schematic of Figure 1 confirms that the software is correctly reconstructing the tomograms. Due to the nature of the shift-and-add algorithm which works by smearing structures that are not on the reconstructed plane, there are various low contrast streaks that are clearly visible on the tomograms. However, the structures that are at a depth of reconstruction are clearly in focus and easily identifiable. In particular, the two washers that overlap in the portal taken at an angle of 0° can be resolved as being located at levels -1 and +1 based on the tomograms of Figures 3a and 3c.

Phantom configuration 2

The coronal and sagittal sections of Figures 4 and 5 show that DTS can be correctly used to determine the correct slice in which markers are positioned. A major difference between the CT and DTS images is that out-of-plane structures are still present in DTS-based tomograms. The pixel shifting property of the chosen reconstruction algorithm is also made apparent by the set screws that are not located in the plane of reconstruction. An artifact shows itself in the form of tracks made by these objects which were shifted so that they do not overlap after the addition of all shifted images. However, any structure on the plane of reconstruction is shifted just enough to remove the parallax shift so that they overlap perfectly in the final tomogram.

A visual inspection of Figure 6 reveals no immediate difference between the tomograms generated from images acquired using a single MU and those acquired using 5 MU even though the original images acquired with 1 MU showed more noise than the ones acquired with the higher dose. This is most likely due to the averaging that happens when shifted images are added in the end.

The inherent low contrast of MV portal images, which makes the localization of markers challenging, is also clearly shown in Figure 6. In this experiment, the proposed solution of manually increasing the contrast produced final tomograms with higher contrast as expected. However, an automatic way to do this

should be found in the future to make the process more streamlined.

Phantom configuration 3

The third phantom was created with much smaller metallic markers present which allowed for testing to be done on the accuracy of the depth information obtained when using DTS based on the shift-and-add algorithm. The 3 CT slices shown in Figure 7 were chosen to represent the CT slice that has the highest intensity for the marker and the first 2 slices on both sides which did not contain any seed information. Figure 8 show various images reconstructed using at 1 mm interval. The DTS image reconstructed at -2.0 cm definitely shows that the seed is present on that tomogram. However, when we reconstructed the tomograms at -1.8 cm and -2.3 cm, an observer may still conclude that the seed is present at these depths. It is only at a depth of -1.5 cm and 2.5 cm that there is enough of a deviation to assume that the seed is not present. For the sagittal reconstructions, the same phenomenon is observed where tomograms reconstructed at depths where the CT shows complete absence of the seed can still be interpreted as containing the seed.

While DTS is known to produce images with much better resolution in the plane of reconstruction as compared to the perpendicular planes [31], there are also some further sources of uncertainty involved in this experiment. As previously mentioned, the location of each seed was manually highlighted to overcome the problem of low contrast seen in the original portal images. It may be that we inadvertently highlighted some pixels which did not receive the signal from the seed, which would cause an artificial shift to be introduced, leading to incomplete overlap of the signal. We also did not perform a correction of the center of rotation, instead depending on the corrections automatically applied to each image from data obtained during the monthly quality assurance checks for the EPID. Finally, there is definitely a certain amount of observer-dependence in deciding whether a particular object is located at a particular depth by assessing the signal for overlap.

The dose delivered to the patient for acquiring the images is comparable to what would be used for portal verification. The time of acquisition slightly increased but the acquisition process could potentially be automated. The calculation time for the data set is of the order of seconds on a PC with an AMD dual-core processor with nominal speed of 1.9 GHz and 2 GB of memory. Thus, with minimal extra effort and time, we would gain a 3D tomographic dataset instead of 2D projection images for the purposes of patient alignment.

Conclusions

The purpose of this work was to determine the feasibility of using the technique of DTS to generate tomograms based on portal images acquired using a gantry-mounted CCD-based EPID. We have demonstrated that, while the tomograms are not of CT quality, we can obtain enough information to determine depth localization information with a 5 mm precision, which is analogous to setting the slice thickness to 5 mm in a CT study. While this is not adequate for any stereotactic application, the current implementation has several sources of error which challenge more precise depth localization. We believe that this precision could be brought down with pre-processing of the source images to get rid of any geometrical artifacts associated with image acquisition.

Given the low contrast inherent to MV quality images, it is not surprising that the final tomograms do not provide a lot of contrast, even in highly bony regions like the head. Work is currently being done to investigate if the different reconstruction algorithms perform the same way with MV quality images. This will also allow us to determine whether the other reconstruction algorithms produce tomograms with better depth resolution.

However, we believe that our results have, at the very least, proved that the use of tomographic data for patient alignment is not limited to centers with the most up-to-date equipment but can also be achieved using a software implementation as long as the center has a portal imaging device.

Acknowledgements

The authors wish to express their gratitude to Tyler Beevers of Civco Medical Solutions for providing the gold seed markers used as part of this project.

References

1. Kupelian P, Willoughby T, Mahadevan A et al. Multi-institutional clinical experience with the Calypso System in localization and continuous, real-time monitoring of the prostate gland during external radiotherapy. Int J Radiat Oncol Biol Phys 2007; 67: 1088-1098.
2. de Crevoisier R, Lagrange JL, Messai T et al. Prostate localization systems for prostate radiotherapy. Cancer Radiother 2006; 10: 394-401.

3. Willoughby TR, Kupelian PA, Pouliot J et al. Target localization and real-time tracking using the Calypso 4D localization system in patients with localized prostate cancer. Int J Radiat Oncol Biol Phys 2006; 65: 528-534.
4. Lefkopoulos D, Ferreira I, Isambert A et al. Present and future of the image guided radiotherapy (IGRT) and its applications in lung cancer treatment. Cancer Radiother 2007; 11: 23-31.
5. Sorcini B, Tilikidis A. Clinical application of image-guided radiotherapy, IGRT (on the Varian OBI platform). Cancer Radiother 2006; 10: 252-257.
6. Perkins CL, Fox T, Elder E, et al. Image-guided radiation therapy (IGRT) in gastrointestinal tumors. J Pancreas (on line) 2006; 7: 372-381.
7. Saw CB, Heron DE, Huq MS et al. Target delineation and localization (IGRT)-part 1. Med Dosim 2006; 31: 1-2.
8. Song WY, Schaly B, Bauman G et al. Evaluation of image-guided radiation therapy (IGRT) technologies and their impact on the outcomes of hypofractionated prostate cancer treatments: a radiobiologic analysis. Int J Radiat Oncol Biol Phys 2006; 64: 289-300.
9. Midgley S, Millar RM, Dudson J. A feasibility study for megavoltage cone beam CT using a commercial EPID. Phys Med Biol 1998; 43: 155-169.
10. Sillanpaa J, Chang J, Mageras G et al. Developments in megavoltage cone beam CT with an amorphous silicon EPID: reduction of exposure and synchronization with respiratory gating. Med Phys 2005; 32: 819-829.
11. Pouliot J, Bani-Hashemi A, Chen J et al. Low-dose megavoltage cone-beam CT for radiation therapy. Int J Radiat Oncol Biol Phys 2005; 61: 552-560.
12. Ford EC, Chang J, Mueller K et al. Cone-beam CT with megavoltage beams and an amorphous silicon electronic portal imaging device: potential for verification of radiotherapy of lung cancer. Med Phys 2002; 29: 2913-2924.
13. Partridge M, Evans PM, Mosleh-Shirazi MA. Linear accelerator output variations and their consequences for megavoltage imaging. Med Phys 1998; 25: 1443-1452.
14. Brenner DJ, Hall EJ. Computed tomography-an increasing source of radiation exposure. N Engl J Med 2007; 357: 2277-2284.
15. Ziedses des Plantes BG. Eine neue methode zur differenzierung in der roentgenographie (planigraphie). Acta Radiol 1932; 13: 182-192.
16. Garrison JB, Grant DG, Guier WH et al. Three dimensional roentgenography. Am J Roentgenol Radium Ther Nucl Med 1969; 105: 903-908.
17. Miller ER, McCurry EM, Hruska B. An infinite number of laminagrams from a finite number of radiographs. Radiology 1971; 98: 249-255.
18. Grant DG. Tomosynthesis: a three-dimensional radiographic imaging technique. IEEE Trans Biomed Eng 1972; 19: 20-28.
19. Dobbins JT 3rd, Godfrey DJ. Digital x-ray tomosynthesis: current state of the art and clinical potential. Phys Med Biol 2003; 48: R65-106.
20. Suryanarayanan S, Karellas A, Vedantham S et al. Comparison of tomosynthesis methods used with digital mammography. Acad Radiol 2000; 7: 1085-1097.
21. Rakowski JT, Dennis MJ. A comparison of reconstruction algorithms for C-arm mammography tomosynthesis. Med Phys 2006; 33: 3018-3032.
22. Wu T, Stewart A, Stanton M et al. Tomographic mammography using a limited number of low-dose cone-beam projection images. Med Phys 2003; 30: 365-380.
23. Zhang Y, Chan HP, Sahiner B et al. A comparative study of limited-angle cone-beam reconstruction methods for breast tomosynthesis. Med Phys 2006; 33: 3781-3795.
24. Zeng K, Yu H, Zhao S et al. Digital tomosynthesis aided by low-resolution exact computed tomography. J Comput Assist Tomogr 2007; 31: 976-983.
25. Yan H, Ren L, Godfrey DJ et al. Accelerating reconstruction of reference digital tomosynthesis using graphics hardware. Med Phys 2007; 34: 3768-3776.
26. Godfrey DJ, Ren L, Yan H et al. Evaluation of three types of reference image data for external beam radiotherapy target localization using digital tomosynthesis (DTS). Med Phys 2007; 34: 3374-3384.
27. Godfrey DJ, Yin FF, Oldham M et al. Digital tomosynthesis with an on-board kilovoltage imaging device. Int J Radiat Oncol Biol Phys 2006; 65: 8-15.
28. Pang G, Bani-Hashemi A, Au P et al. Megavoltage cone beam digital tomosynthesis (MV-CBDT) for image-guided radiotherapy: a clinical investigational system. Phys Med Biol 2008; 53: 999-1013.
29. Descovich M, Morin O, Aubry JF et al. Characteristics of megavoltage cone-beam digital tomosynthesis. Med Phys 2008; 35: 1310 - 1316.
30. Kolitsi Z, Panayiotakis G, Anastassopoulos V et al. A multiple projection method for digital tomosynthesis. Med Phys 1992; 19: 1045-1050.
31. Bachar G, Siewerdsen JH, Daly MJ et al. Image quality and localization accuracy in C-arm tomosynthesis-guided head and neck surgery. Med Phys 2007; 34: 4664-4677.